Chapter 4

Fabrication and Measurement

4.1 Introduction

Our module was designed and analyzed in previous chapter. The optimum design to achieve 1 μm spot size was obtained and the tolerance of 3 μm lateral offset, 9 degree angular tilt were achieved.

In this chapter, the module was fabricated and the fabrication process will be presented in next section. The intensity distributions and spot size from fiberlens and that after SIL were measured, presented and compared with simulation.

4.2 Fabrication

Our module includes fiberlens, SIL and V-groove. The fabrication of fiberlens and V-groove was reported by Chung-Hao Tien [1] and Meng-Yu Wu [2] so here the fabrication of SIL is discussed. The SIL is fabricated by Yu-Ru Chang in Prof. Wen-Syang Hsu laboratory.

Generally, the aperture is made prior to the SIL. But the misalignment between SIL and aperture occurs during the discrete pattern processes. In order to solve it, we proposed a backside exposure process to fabricate SIL aligned with aperture, as shown in Fig. 4-1. First, the Ti film is deposited as the sacrificial layer. The α-Si pedestal and Ni seed layer is made by lift-off process. The Ti film is undercut by chemical wet etching. The center gap is defined as our aperture and the other opening gap is used to define the radius of SIL for backside exposure. The pattern of

photoresister (AZ-4620) is self-aligned by backside exposure. SIL is fabricated by thermal reflow process.

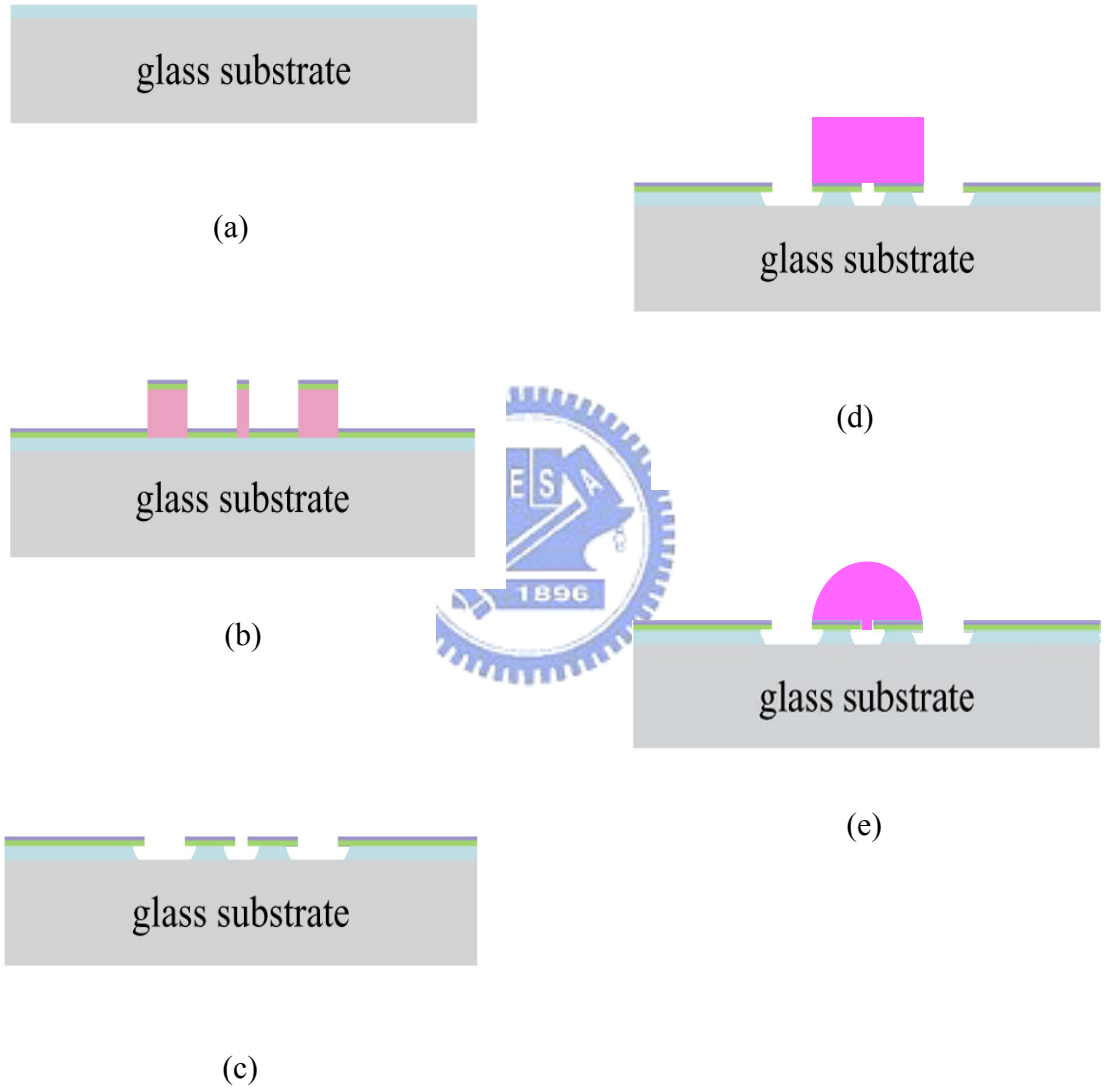

Fig. 4-1 Fabrication process of SIL with aperture; (a) Step 1: Deposit Ti layer, (b) Step 2: Deposit α - Si and Ni layer, (c) Step 3: Undercut Ti layer, (d) Step 4: Backside exposure and (e) Step 5: Reflow

This method defines radius of SIL by the aperture layer so the misalignment with aperture and SIL will not occur. Although the method limits the radius of SIL due to the resolution of the mask and exposure equipment, we choose the above method to fabricate SIL with aperture because misalignment is a highly challenge issue in SIL with aperture module. However the maximum radius is limited by the thickness and absorption of SIL.

4.2.1 Fabrication results

First, we consider the SIL without aperture. The curvature of reflow structure is determined by the aspect ratio, surface tension and reflow process. In order to obtain the SIL with precise dimension, a group of patterns with different aspect ratio was reflowed with the same process parameters and measured via SEM. The thickness was kept 25 μ m, while the diameter of circular patterns varied from 20 μ m to 50 μ m to generate the aspect ratio from 0.5 to 1.25.

After the reflow process, the dimension changed. The result was summarized in Table 4-1. In case 1 with aspect ratio of 1.25, shown in Fig. 4-2(a), the diameter increased but the height decreased dramatically. It showed that the surface tension can not support the super-hemisphere. This means that SSIL can not be formed by using AZ-4620.

In case 2 with aspect ratio of 0.5, as shown in Fig. 4-2(b), the diameter and height decreased 4% and 10% respectively. A precise hemisphere can be generated by compensating the variations of thickness and diameter.

According to the results, a hemispherical SIL was fabricated, as shown in Fig.4-3. The SEM photograph is shown in Fig. 4-4. The larger circle is used for backside

exposure and the SIL is located at the center.The dimension and curvature of hemisphere can be precisely controlled.

Table 4-1 Dimension variation

	Case 1	Case 2
Height	-26.3%	-3.4%
Radius	+7.2%	-9.4%

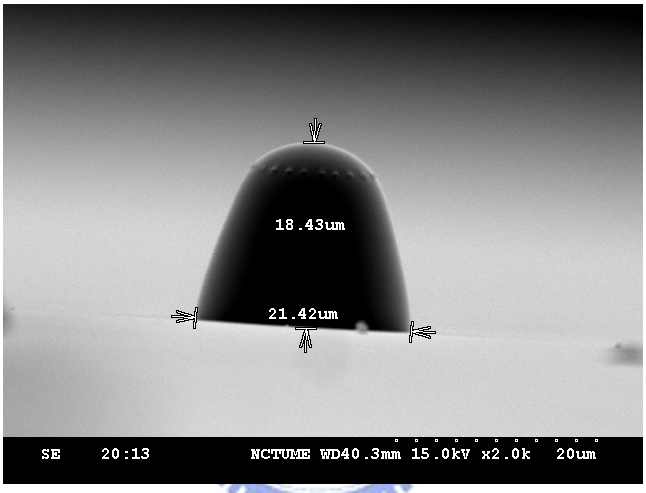

(a)

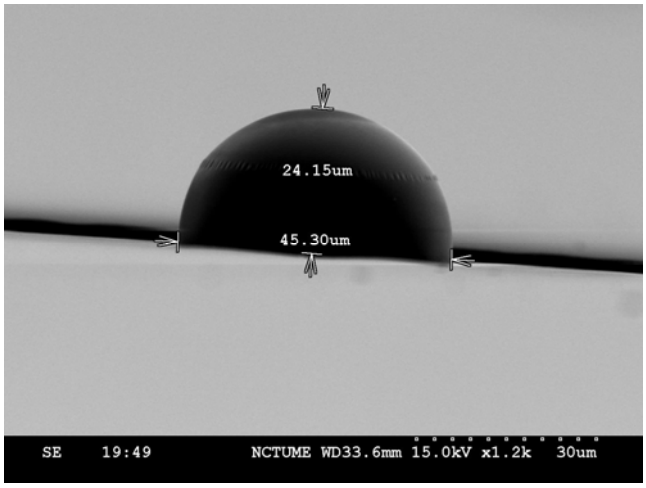

(b)

Fig. 4-2 SEM of SIL @ aspect ratio (a) 1.25 and (b) 0.5

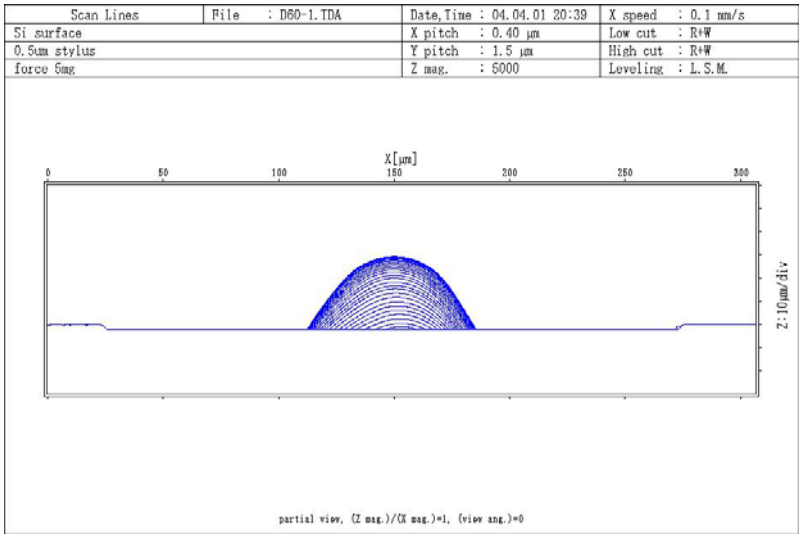

Fig. 4-3 30 μ m radius SIL profiles

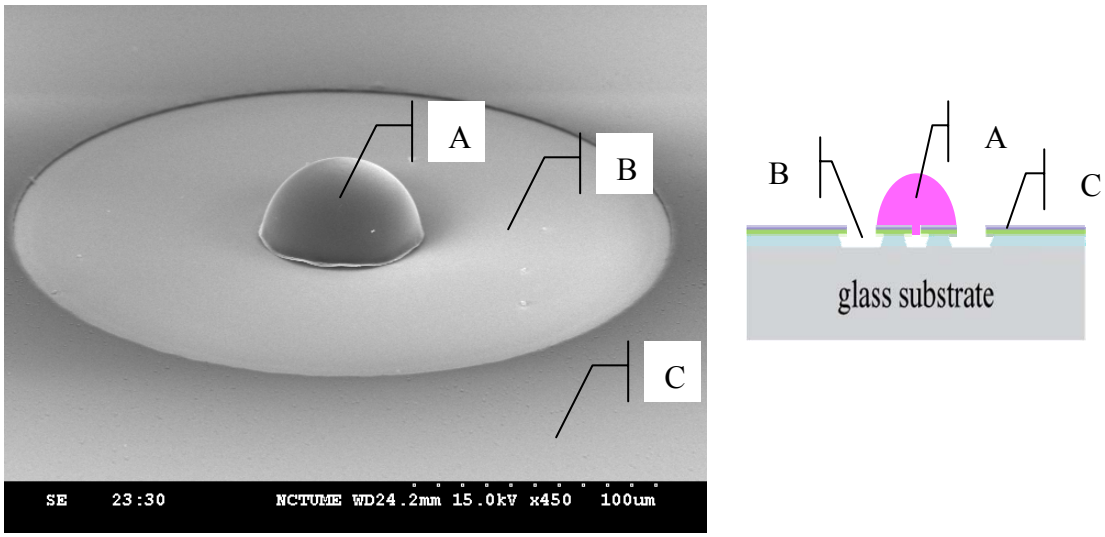

Fig. 4-4 SEM of SIL with aperture

4.3 Measurement

Compared with the pixel size of CCD camera typically 5μm to 10μm, the focused spot size of the module, which is less than 3μm from previous simulation, is too small to be recognized by CCD. A co-focal system was used to broaden the output beam for the measure meat of the spot size, as shown in Fig.4-5.

The incident beam passes through our module and is focused between our module and objective lens. The output beam from objective lens will be collimated when the focused spot is positioned in the focal plane of the objective lens. Finally, the output beam is detected by CCD camera. The output beam size is defined as full-width at $1/e^2$ maximum intensity, as shown in Fig.4-6.

This method results in the output beam larger than diffractive limit and does not need precisely control the position of the objective lens and CCD camera. In order to ensure that the output beam is collimated, the spot size is measured and should be remained the same at several positions which are far from the objective lens.

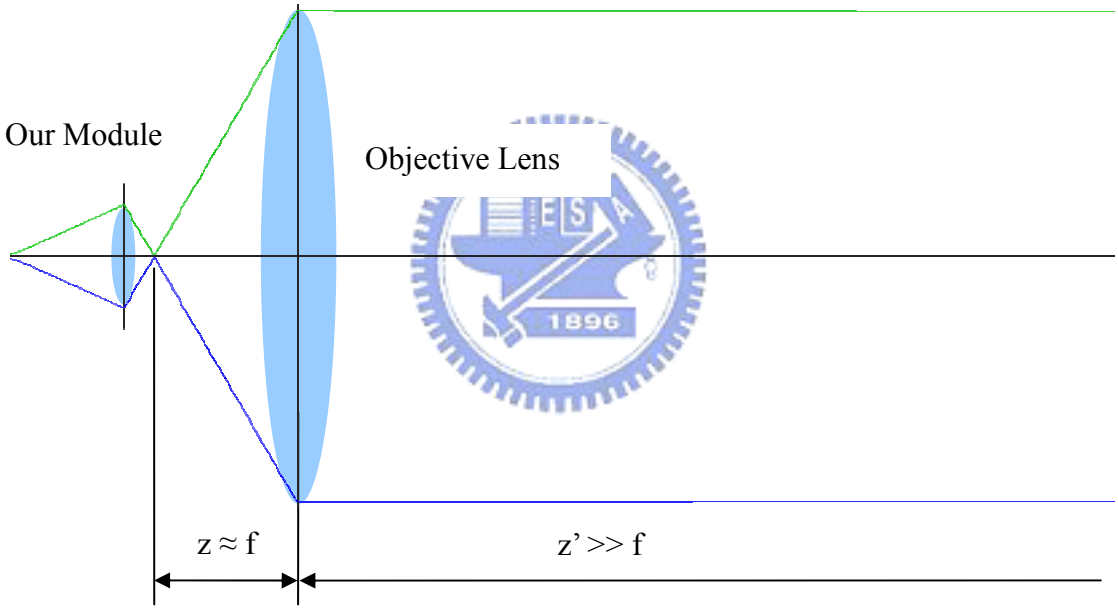

Fig. 4-5 Measuring System Setup

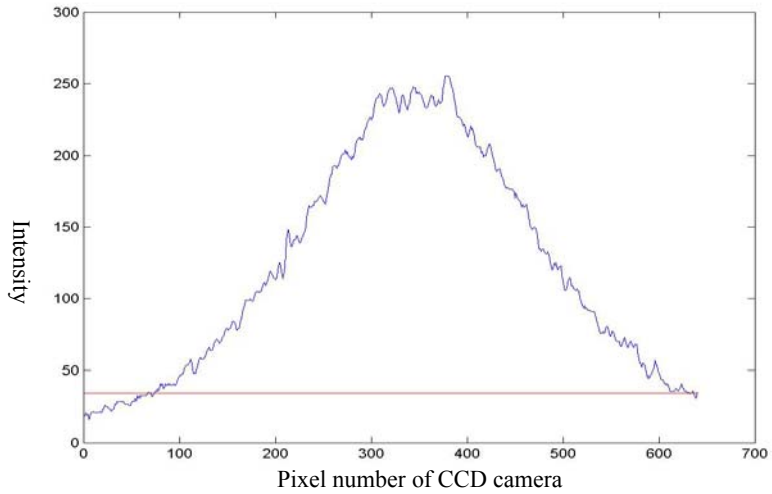

Fig. 4-6 Definition of output beam size

What we really measured was the collimated output beam size but not the focused spot size which we want to know. Therefore, we use the Gaussian beam condition to calculate spot size according to fundamentals of photonics [3].

4.3.1 Principle

If a lens is placed at the waist of a Gaussian beam, as shown in Fig. 4-7, the transmitted beam is then focused to a waist radius W_0' at a distance z' given by

$$W_0' = \frac{W_0}{[1+(z_0/f)^2]^{1/2}} \qquad (4\text{-}1)$$
$$z' = \frac{f}{1+(f/z_0)^2}$$

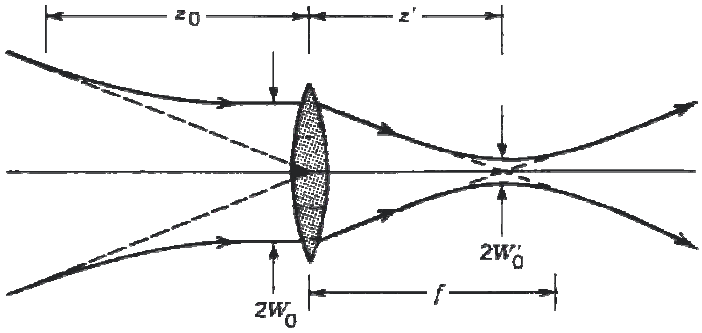

Fig. 4-7 Focusing a beam with a lens at the beam waist

If the depth of focus of the incident beam $2z_0$ is much longer than the focal length f of the lens (Fig. 4-5), then $W_0' \approx (f/z_0)W_0$. Using $z_0 = \pi W_0^2/\lambda$, we obtain

$$W_0' = \frac{\lambda}{\pi W_0} f = \theta_0 f \qquad (4\text{-}2)$$
$$z' = f$$

The transmitted beam is then focused at the lens' focal plane as would be expected for parallel rays incident on a lens. This occurs because the incident Gaussian beam is well approximated by a plane wave at its waist. The spot size expected from ray optics is, of course, zero. In wave optics, however, the focused waist radius W_0' is directly proportional to the wavelength and the focal length, and inversely proportional to the radius of the incident beam.

In our condition, it is desirable to generate the smallest possible spot size. It is clear from equation (4-2) that this may be achieved by use of the shortest possible wavelength, the thickest incident beam, and the shortest focal length. Since the lens should intercept the incident beam, its diameter D must be at least $2W_0$. Assuming that $D=2W_0$, the diameter of the focused spot is given by

$$2W_0' \approx \frac{4}{\pi}\lambda F\# \qquad (4\text{-}3)$$
$$F\# = \frac{f}{D}$$

where F# is the F-number of the lens. A microscope objective with small F-number is often used. Since equation (4-2) is approximate, their validity must always be confirmed before use.

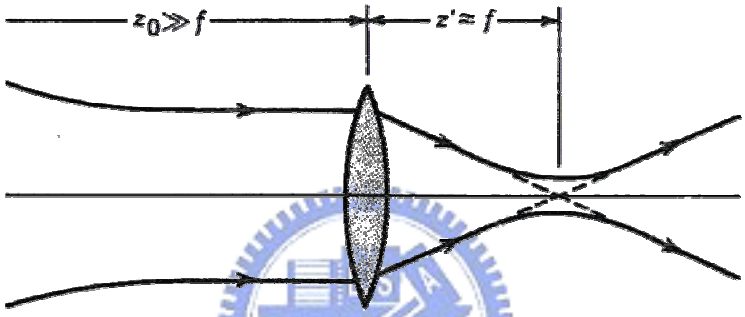

Fig. 4-8 Focusing a collimated beam

4.3.2 Measurement equipments

According the misalignment analyses, the resolution of the stage should be less than of 3 μm. Therefore, we choose a 3-axial position stage with the resolution of 0.5 μm to make sure the component aligned with each other. The specification of CCD camera is shown in Table 4-2. In order to improve the accuracy, the sensing area of CCD camera is square and the spot diagraph is captured by capture card without compression. Then we wrote a Matlab program to get the profile of the spot and analyze the spot size.

Since we assumed that the ambient light has an influence on our measurement,

the intensity of ambient light was measured, as shown in Fig. 4-9. Because the intensity of ambient light is much smaller than the intensity of spot, the ambient light is used as the background noise to correct the measured data.

Table 4-2 Specification of CCD camera

Pick-up device	1/3 type CCD
Effective picture elements	659(H) X 497(V)
Sensing area	7.4μm X 7.4μm
Horizontal frequency	15.734 kHz
Vertical frequency	59.94 Hz

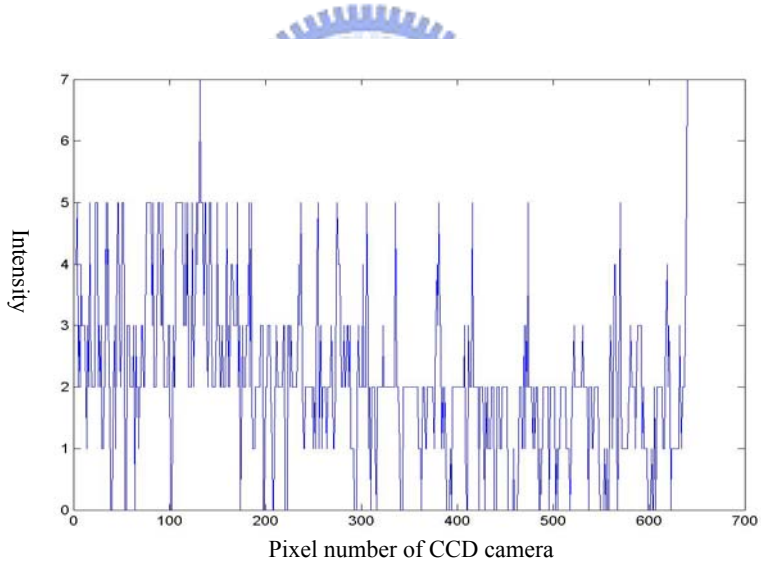

Fig. 4-9 Intensity of ambient

4.3.3 Fiberlens measuring setup

In order to compare with simulation, the spots emitted from the fiberlens were measured and verified. A 633nm laser is coupled into fiber. A 3-axial position stage is used to control the distance between fiberlens and objective lens. A CCD camera is put on the guider and is adjusted the position from 12cm to 32cm toward objective lens. Compared with the focal length of objective lens is 1.6cm, the distance between objective lens and CCD camera is much larger than the focal length of objective lens. The output beam can be approximated as a collimated beam when the spot size on the CCD camera remains the same in different positions. According to equation (4-3), the spot size was calculated. The measuring system of fiberlens is shown in Fig.4-10.

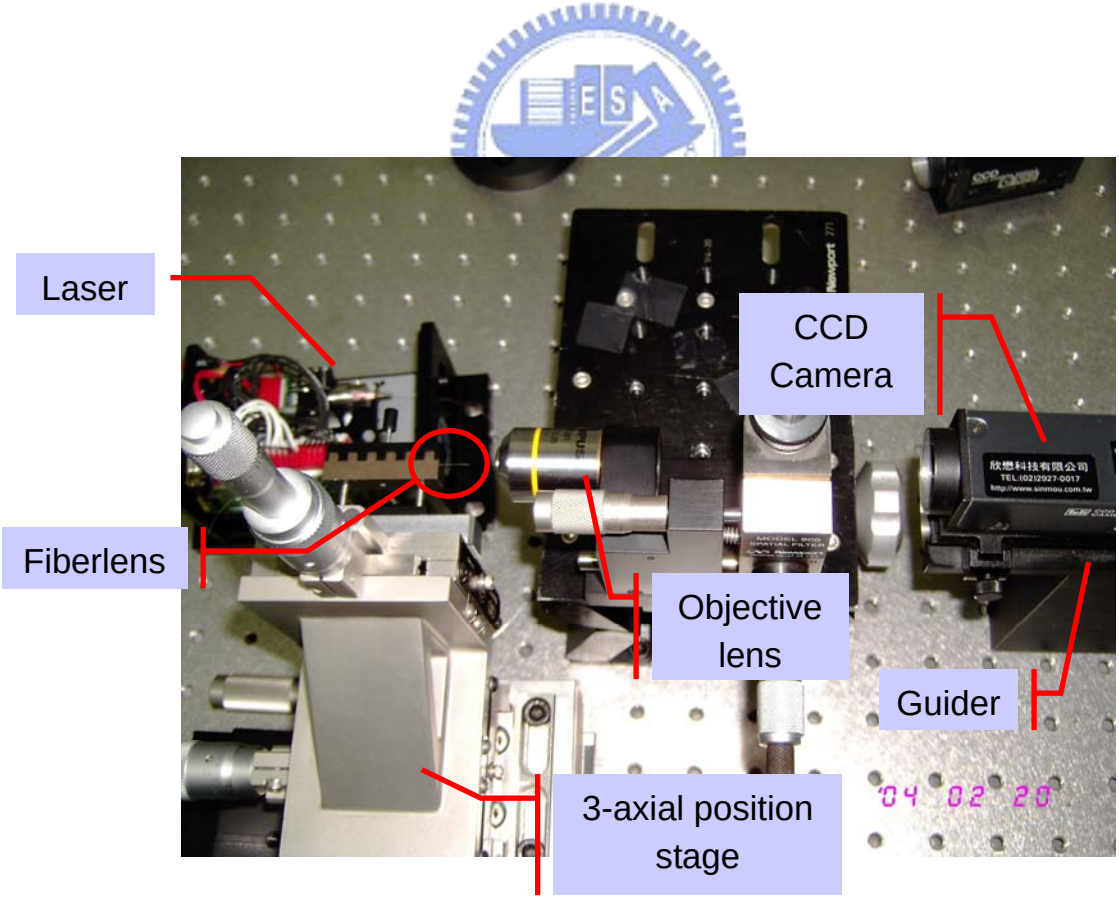

Fig. 4-10 Photograph of the fiberlens measuring system

4.3.4 Fiberlens & Solid Immersion Lens measuring setup

The previous system was modified to measure the properties of spot from fiberlens and SIL. The 3-axial position stage (2) is added to control the position of SIL. CCD camera (2) is used to capture the distance between fiberlens and SIL. The position of objective lens is adjusted to make the output beam collimated. The optimum position of SIL is determined according to the spot size which captures from CCD camera (1). Finally, the final output beam was computed by the equation (4-3). The measurement system of fiberlens and SIL is shown in Fig.4-11.

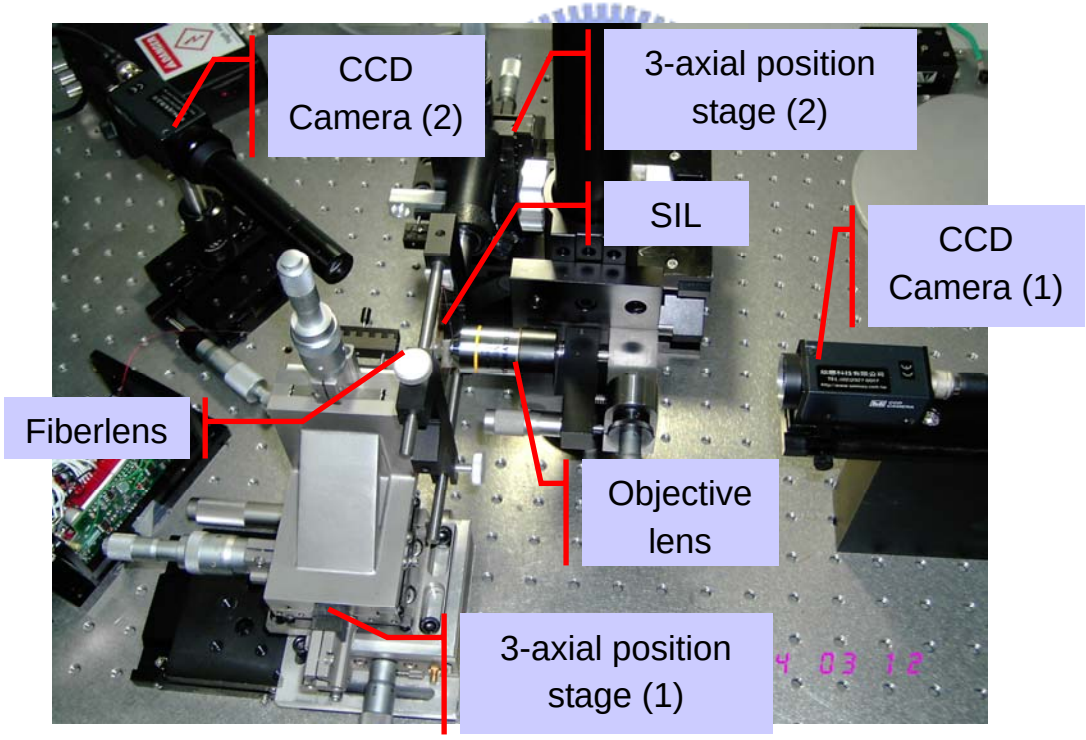

Fig. 4-11 Photograph of the fiberlens plus SIL measuring system

4.3.5 Measurement results

We fabricated different length of fiberlens and used microscope to measure the length of fiberlens precisely. The measurement results are shown in Fig. 4-12. Corresponding to the simulation results, the trends of measurement and simulation are similar. Obviously, the variations of NA increases as the fiberlens length increase and the variations of spot size decrease as the fiberlens length increases. The measurement results agree with the simulation.

However, by comparing the measurement with simulation, some deviations, caused from the variation of radius of fiberlens, were found. We also found the limitation of fiberlens length is about 1000μm not 820μm from simulation. Therefore, we suspected the radius of fiberlens isn't ideal. In ideal cases, radius of fiberlens was assumed 62.5μm which is equal to the radius of single mode fiber, but actually it is larger than 62.5μm due to the surface tension. From the measured NA and spot size compared with the simulation, the real radius of fiberlens is estimated around 72.5μm. The shape of fiberlens was 70.5μm which was measure by the CCD camera, as shown in Fig. 4-13. This result also explain why the limitation of fiberlens length is about 1000μm not 820μm from simulation.

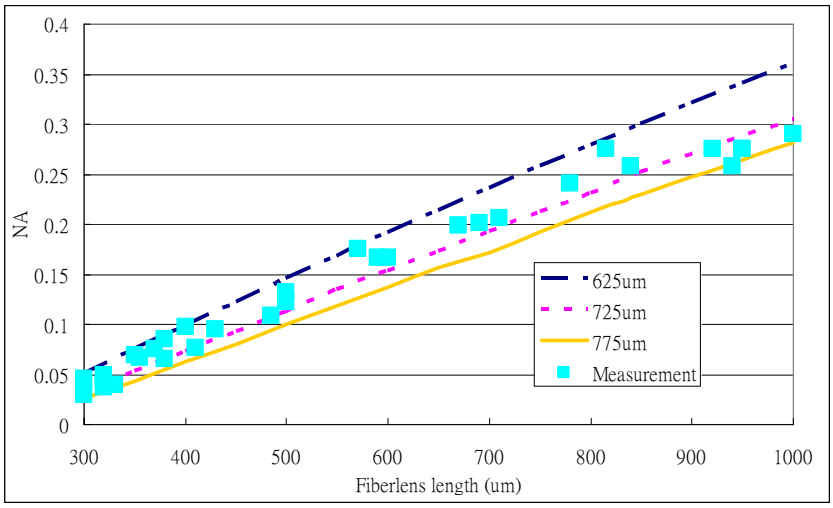

(a)

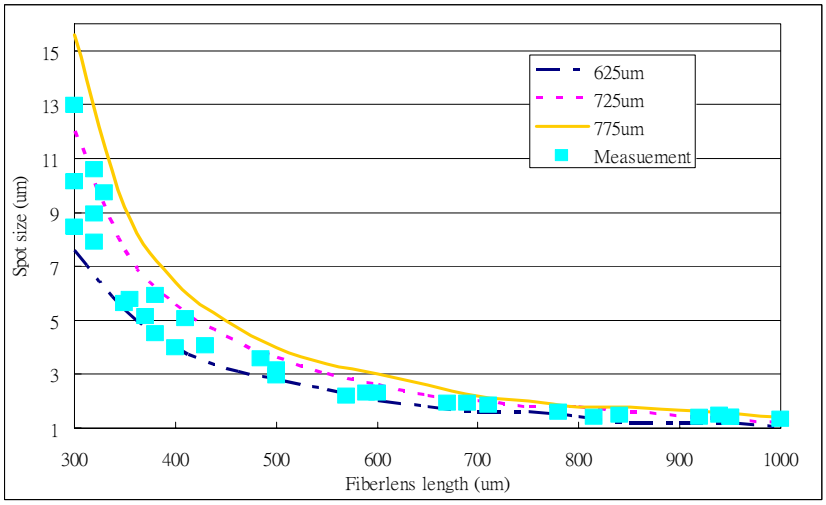

(b)

Fig. 4-12 Fiberlens length vs. (a) NA and (b) Spot size

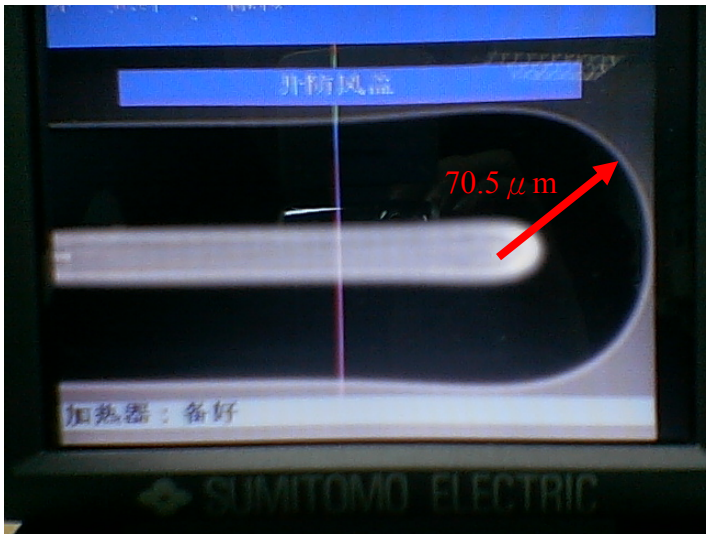

Fig. 4-13 Photograph of fiberlens

Two kinds of SIL were fabricated to verify our simulation, as shown in Fig. 4-14. The fiberlens length we used is 650 μ m and the beam profile is shown in Fig. 4-15. The spot size is 2.99 μ m and NA is 0.2.

In condition A, the SIL is 30 μ m in radius and 30 μ m in thickness, as shown in Fig. 4-14(a). The output beam profile is shown in Fig. 4-16. The measured spot size is 2.09 μ m and NA is 0.28. However, the calculated spot size is 1.67 μ m.

In condition B, the SIL is 35.2 μ m in radius and 31.5 μ m in thickness, as shown in Fig .4-14(b). The output beam profile is shown in Fig. 4-17. The spot size is 2.12 μ m and NA is 0.28. However, the spot size is 1.82 μ m by simulation.

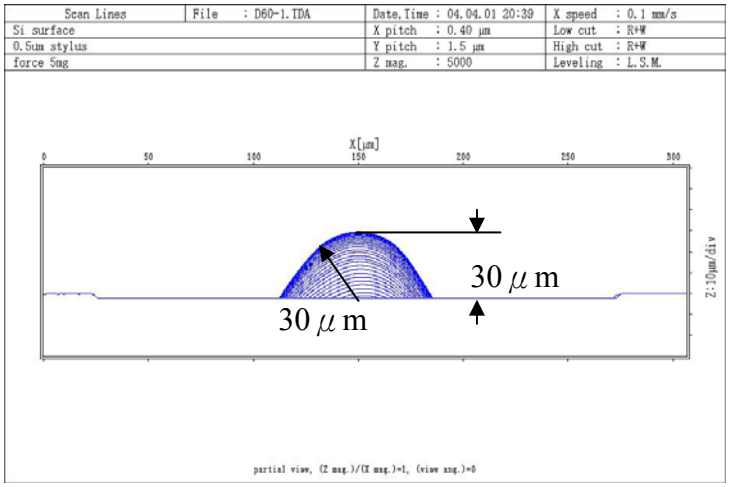

(a)

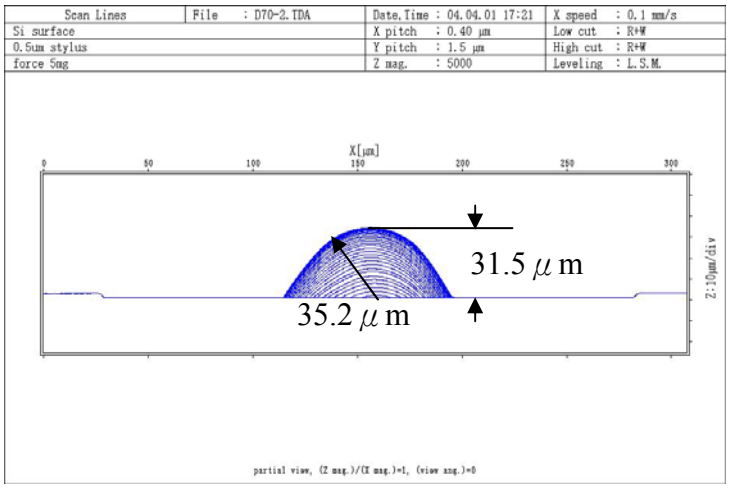

(b)

Fig. 4-14 (a) 30 μ m and (b) 35.2 μ m radius SIL profiles

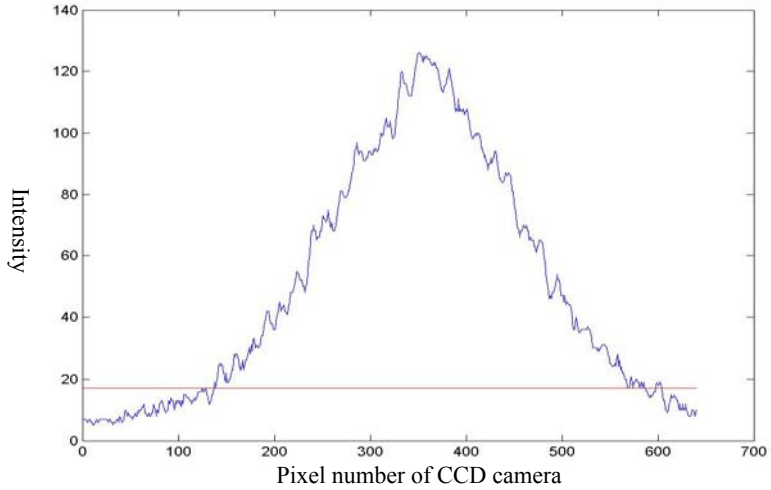

Fig. 4-15 Beam profile of 650 μ m fiberlens

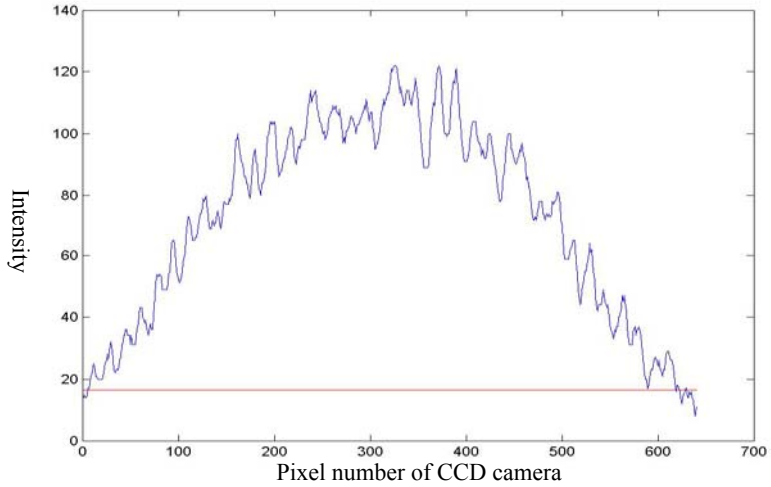

Fig. 4-16 Beam profile of 650 μ m fiberlens with 30 μ m radius SIL

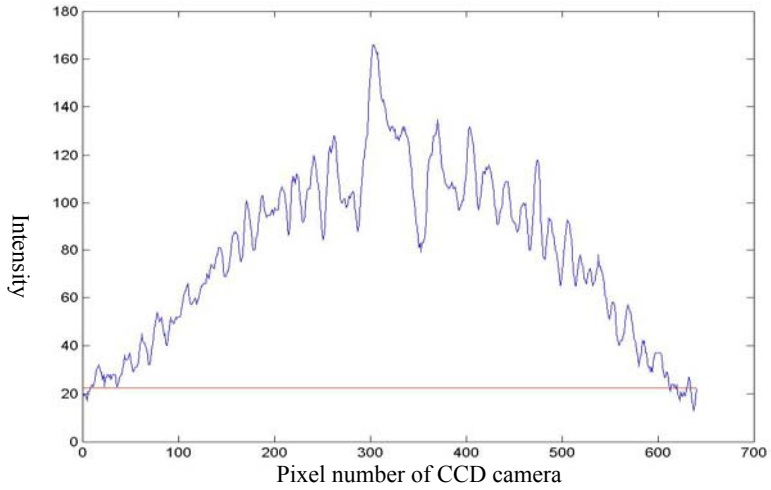

Fig. 4-17 Beam profile of 650 μ m fiberlens with 35 μ m radius SIL

The different between simulation and measurement may be caused by the measurement error, aberration and the refractive index of SIL. The measurement error is mainly caused from the error of the collimated beam size. The error of spot size and NA can be calculated by the equation (4-3). The error of spot size is $\pm$ 0.1 μm and the error of NA is $\pm$ 0.013.

Because the beam size is too large compared with the radius curvature of fiberlens, the periphery of the beam can not viewed as the paraxial beam. Therefore, the spherical aberration occurs and becomes more serious as the fiberlens length increase. We used Diffract ™ to evaluate the Seidel coefficient, as shown in Fig.4-18. The spot size ratio is defined as the ratio of the spot size to the spot size without aberration. Obviously, as Seidel coefficient increases, the spot size ratio increases, too. When the Seidel coefficient is close to 1 λ, the spot size variation becomes saturated.

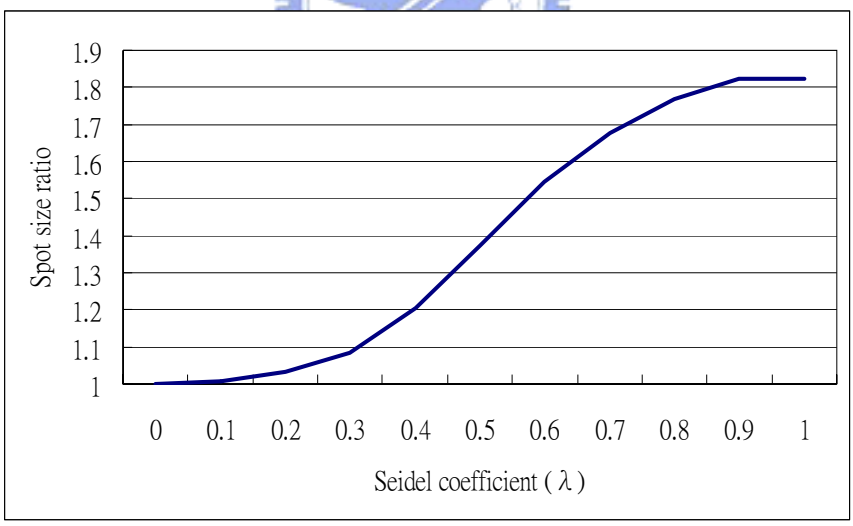

Fig. 4-18 Seidel coefficient vs. spot size ratio

The refractive index of photoresister, AZ-4620, is from 1.6 to 2.0 due to the thickness variation and different thermal process [5]. The fiberlens plus SIL model in Chapter 3 is used to simulate the spot size as the refractive index of SIL varies. The

relation between spot size and refractive index of SIL is shown in Fig.4-19. The Seidel coefficients with our condition were evaluated by Zemax. The Seidel coefficients is 0.24, so spot size ratio is 1.05 from Fig.4-18. We can obtained the refractive index of 30 μ m to be 1.58 and the refractive index of 35 μ m to be 1.69 when we assume that the measurement error was -0.1 μ m and the Seidel coefficients was 0.24. The results shows that the refractive index of AZ-4620 is sensitive to the thickness variation and different thermal process.

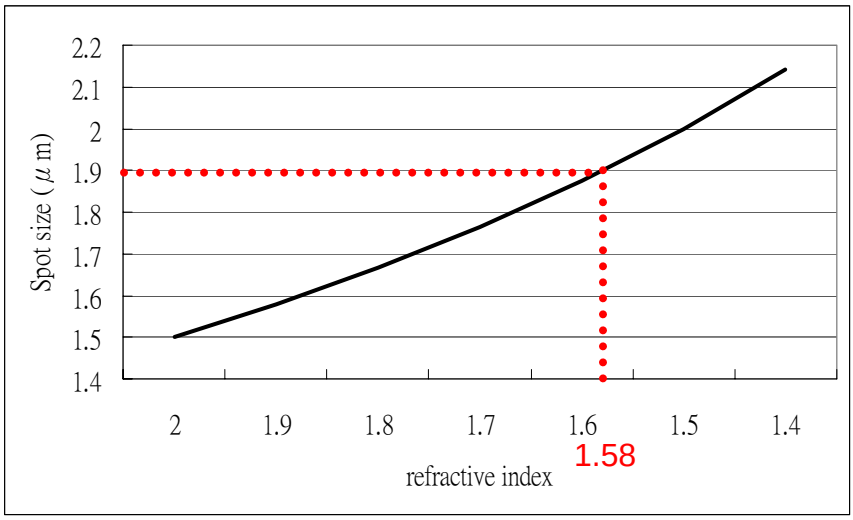

(a)

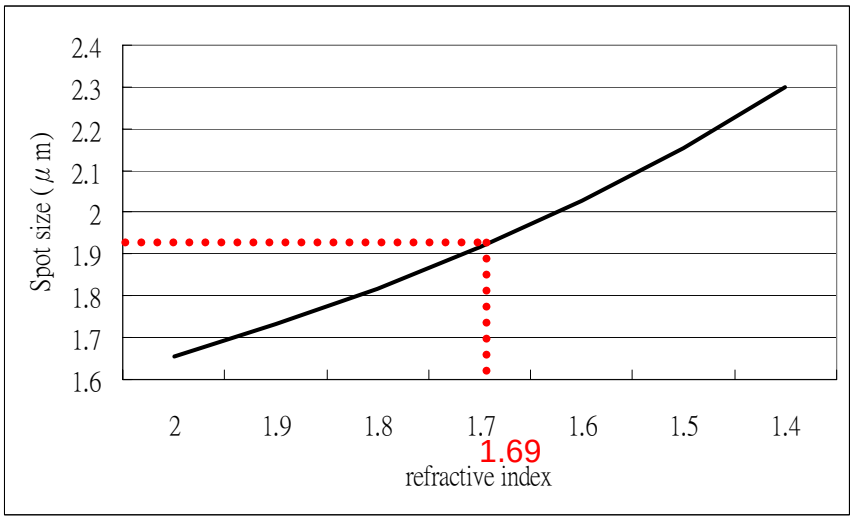

(b)

Fig. 4-19 The refractive index of (a) 30 μ m and (b) 35.2 μ m radius SIL vs. spot size

4.4 Summary

The fiberlen and SIL were fabricated and the measurement system was established. The principle of measurement system was presented and the criteria of it were discussed. Because the radius of fiberlens is around 72.5μm not 62.5μm in ideal, the limitation of fiberlens is 1000μm not 820μm from simulation. The different between simulation and measurement may be caused by the refractive index of SIL, aberration and the measurement errors. The refractive index of 30 μ m is 1.58 and the refractive index of 35 μ m is 1.69 as we assume that the measurement error is -0.1 μ m and the Seidel coefficients is 0.24. The refractive index of AZ-4620 is sensitive to the thickness variation and different thermal process. The measurement results also certify that the module which includes fiberlens, V-groove and SIL is performed.